RSC Advances

PAPER

Check for updates

Cite this: *RSC Adv.*, 2021, **11**, 19395

Novel fabrication of a yeast biochar-based photothermal-responsive platform for controlled imidacloprid release†

Meng Mei,[ab] Bo Bai,[abcd]* Dan Zheng,[ab] Na Hu[cd] and Honglun Wang[cd]

For improving the utilization efficiency of pesticides, we developed a novel pesticide delivery particle (YINCP@EC) with a core–shell structure based on yeast biochar, imidacloprid (IMI), ammonium bicarbonate (NH_4HCO_3), calcium alginate (CA), and ethyl cellulose (EC). Therein, yeast biochar, IMI and NH_4HCO_3 were absorbed in the network-structured of CA to obtain YINCP through hydrogen bonds. The resulting composite was granulated using an ion gelation technique and then coated with EC to form YINCP@EC. In this platform, yeast biochar serving as a photothermal agent can efficiently convert sunlight energy into thermal energy, thereby triggering NH_4HCO_3 decomposition into CO_2 and NH_3 that can break through the EC coating and facilitate IMI release. In addition, the influence of yeast biochar content, pH, and coexisting ions was systematically studied to evaluate the release behavior of IMI from YINCP@EC. Moreover, the hydrophobic EC shell endowed YINCP@EC with high stability in aqueous solution for at least 60 days. Consequently, this novel composite with simple preparation, low cost and remarkable photothermal-responsive properties has a huge application potential in agriculture.

Received 18th March 2021
Accepted 22nd May 2021

DOI: 10.1039/d1ra02143e

rsc.li/rsc-advances

1. Introduction

Pesticides have made great contributions to agriculture by protecting crops from weeds, pests, diseases and fungus, and nearly one-third of the world's food production may be reduced without pesticide application.[1–5] Nonetheless, as much as 90% of the applied conventional pesticides are unable to reach the target organisms and migrate into the environment *via* volatilization, run-off, and leaching, which result in an increase in production costs and serious environmental pollution.[6–9] In recent years, controlled stimuli-responsive release platforms have attracted increasing global commercial and scientific interest for their ability to deliver active ingredients to desired sites in a specified manner.[10–14] In particular, the advantages of controlled stimuli-responsive release platforms of pesticides over conventional modes include (i) extending the duration of pesticide activity,[15] (ii) reducing manpower input,[16] (iii) alleviating environment pollution through minimizing residues,[17,18] and (iv) protecting the active ingredients against environmental degradation.[19,20] Therefore, many investigations on controlled stimuli-responsive release platforms have been conducted to enhance the utilization efficiency of pesticides.[21–24]

Controlled stimuli-responsive release platforms provide advanced and intelligent controlled release of pesticides, where the platforms present responses to external stimuli (like pH,[25] temperature,[26] microbe,[23] and light[24]), resulting in changes in their chemical or physical properties favoring the "on-demand" release of loaded pesticides.[5,7] Among these stimuli-responsive release systems, pH-responsive formulations might affect the growth of crops due to the introduction of acid or base; temperature and microbe responsive formulations displayed high energy-consumption and complex operation. In comparison, photothermal-responsive platforms have the most potential in practical applications since they can directly take advantage of the clean and abundant natural sunlight as a triggering source.[27] In addition, photothermal agents as the core component of photothermal-sensitive platforms were intensively investigated by researchers.[28,29] Until now, several kinds of photothermal-responsive materials including polydopamine,[30] CuS–polydopamine,[31] graphene oxide,[32] *etc.*, have been fabricated for light-triggered pesticides release. However, these nanomaterials have various shortcomings such as potential toxicity, expensive cost, complex manufacturing process and low photothermal conversion efficiency, which greatly affect their expanded application. Thus, it is extremely necessary to construct a novel photothermal-responsive pesticide release platform based on an environmentally safe photothermal agent with the cost-effective, simpler procedure and excellent light-to-heat conversion performance merits.

[a]*Key Laboratory of Subsurface Hydrology and Ecological Effects in Arid Region of the Ministry of Education, Chang'an University, No. 126 Yanta Road, Xi'an 710054, Shaanxi, China. E-mail: baibochina@163.com*

[b]*School of Water and Environment, Chang'an University, Xi'an, 710054, P. R. China*

[c]*Key Laboratory of Tibetan Medicine Research, Northwest Institute of Plateau Biology, Chinese Academy of Sciences, Xining, 810008, China*

[d]*Qinghai Provincial Key Laboratory of Tibetan Medicine Research, Xining, 810001, P. R. China*

† Electronic supplementary information (ESI) available. See DOI: 10.1039/d1ra02143e

This article is licensed under a Creative Commons Attribution-NonCommercial 3.0 Unported Licence.

(cc) BY-NC

© 2021 The Author(s). Published by the Royal Society of Chemistry

The yeast biochar is a low cost photothermal agent because it can be easily prepared through mild hydrothermal treatment of waste yeast, which is abundant in the brewing industry.[33] As a common amorphous carbon, the yeast biochar can naturally absorb broadband wavelength light because of the tightly spaced energy levels arising from the hover ground held π electrons. The excited electrons release heat by relaxing to the ground state after illumination.[34,35] Furthermore, the synthetic yeast biochar possesses a porous structure, which can be used as an ideal carrier for pesticides. Moreover, the cell wall of yeast biochar after mild hydrothermal treatment still has sufficient chemically reactive functional groups inherited from yeast cells, including hydroxyl (–OH), amine ($-NH_2$), carboxyl (–COOH), acylamino ($-CONH_2$) and sulfonyl ($-SO_3H$) groups,[36,37] which can provide prerequisite loading sites for other cargoes through strong hydrogen bonds. Based on the above consideration, the yeast biochar with facile preparation, low cost, biosafety and high light-to-heat conversion efficiency has shown broad prospects in constructing a photothermal-responsive platform for enhancing the utilization efficiency of pesticides. To data, the synthesis of photothermal agent using yeast biochar for controlling the release of pesticides is rarely reported.

Inspired by these backgrounds, we developed an intelligent controlled pesticide release platform (YINCP@EC) *via* the incorporation of yeast biochar, imidacloprid (IMI), ammonium bicarbonate (NH_4HCO_3), calcium alginate (CA) and ethyl cellulose (EC). The core of our innovation is that the yeast biochar-based composite was used as a photothermal-sensitive gatekeeper and a pesticide reservoir. IMI,[38] a frequently-used neonicotinoid insecticide, was chosen as a model pesticide to evaluate the controlled release behaviors of composites due to its wide application in modern agriculture (approximately 11–15% of the total pesticide market). The fabrication process of YINCP@EC and the mechanism of IMI photothermal-responsive release were proposed, and the structural, morphology, photothermal-sensitive properties of the samples were also investigated. The experimental results have confirmed that the as-prepared YINCP@EC exhibited excellent photothermal sensitivity and can control the sustained release of IMI effectively. Based on these properties, the biodegradable and environmentally friendly YINCP@EC may have great potential application in agriculture fields for pesticides effective utilization.

2. Experimental section

2.1. Materials

Yeast powder was brought from Angel Yeast Corp. (Wuhan, China). EC, sodium chloride (NaCl), sodium carbonate (Na_2CO_3) and ethyl alcohol were provided by Xi'an Chemical Reagent Factory (Shaanxi, China). Glutaraldehyde solution (25% v/v), acetone, SA, calcium chloride ($CaCl_2$), NH_4HCO_3, hydrochloric acid (HCl), sodium hydroxide (NaOH), and sodium sulfate (Na_2SO_4) were supplied by Tianjin Chemical Reagent Factory (Tianjin, China). IMI (purity of 95%) was brought from Shanghai Yuanye Bio-Technology Co., Ltd (Shanghai, China). All reagents were used without further purification.

2.2. Synthesis of composites

2.2.1 Synthesis of yeast biochar. The yeast biochar was synthesized by using a mild hydrothermal treatment.[33,39] Typically, 3 g yeast powder was immersed in acetone solution (50 mL) and stirred for 10 h. Then, the supernatant was removed by centrifugation, and washed with deionized water several times to remove excess acetone. Subsequently, the washed yeast powder was added in 2% (v/v) glutaraldehyde solution (50 mL), which was then placed in a Teflon-sealed autoclave (100 mL) and kept at 200 °C for 12 h. After that, the resultant yeast biochar was collected after several washing–centrifugation–redispersion cycles and drying in the oven at 80 °C.

2.2.2 Synthesis of YINCP@EC. The yeast biochar, SA, NH_4HCO_3 and IMI with mass ratios of $W_{\text{yeast biochar}}/W_{\text{SA}}/W_{NH_4HCO_3}/W_{\text{IMI}}$ = 0 : 2 : 4 : 0.5, 1 : 2 : 4 : 0.5, 2 : 2 : 4 : 0.5, 3 : 2 : 4 : 0.5, 4 : 2 : 4 : 0.5, respectively, were evenly mixed in a 50 mL beaker. After that, a certain amount of distilled water was added to the resulting mixtures to form 25 mL mixed solution. Then, the resulting mixture was stirred at 100 rpm at room temperature for 30 min to construct a homogeneous suspension and stewing for 1 h to sufficiently remove the bubble. Afterward, the above mixed solution was added dropwise into a 3% (w/v) $CaCl_2$ aqueous solution using a 0.8 mm gauge syringe without the needle. After hardening for 30 min, the formed beads were filtered out by a net, washed three times with deionized water, and the beads were dried at 20 °C for 24 h to obtain YINCP. Finally, YINCP was soaked in 10 mL of EC ethanol solution (w/w, 5%) for 1 h, taken out, and air drying for 4 h at room temperature to obtain YINCP@EC.

2.3. Characterization

The scanning electron microscope (SEM, Hitachi S-4800) was applied to investigated the surface morphologies of obtained products. The functional groups of the samples were analyzed on a Fourier transform infrared spectrometer (FTIR, PerkinElmer Spectrum Two). The zeta potential of samples was determined by Zetasizer Nano ZS ZEN3700. Thermogravimetric analysis (TGA) was performed at a temperature ranging from 25 to 900 °C on a HENVEN HCT-3 thermogravimetric analyzer. Carry 5000 spectrophotometer was used to obtain UV-vis-NIR spectrum. The sunlight was provided by a xenon lamp (PLS-SXE300C). The temperatures in the tests were measured by using a non-contact infrared thermometer (GM320, BENETECH). The light intensity was measured by an FZ-A radiometer was 100 mW cm^{-2}. Thermal pictures were captured by an infrared camera (CHAUVIN ARNOUX/CA73). The release efficiency of IMI at different solution was determined by Cary 752 N UV-VIS spectrophotometer at a wavelength of 271 nm.

2.4. Stability investigation

YINCP@EC (20 mg) kept steadily in a container with deionized water (5 mL) at room temperature and were filtered after 1, 7, 15, 30 and 60 d, respectively. The weight of the remaining sample was weighed after air drying. Finally, the collapse ratio (CR) of the sample was detected by the following eqn (1):

$$\mathrm{CR} = \frac{W_t}{W_0} \times 100\% \quad (1)$$

© 2021 The Author(s). Published by the Royal Society of Chemistry

where W_t (g) and W_0 (g) are the weight of the sample at time t and initial dried state.

2.5. Measurement of photothermal performance

2.5.1 Photothermal performance of yeast biochar. For assessing the photothermal conversion performance of the synthesized yeast biochar, a cuvette (4 mL) containing 2 mL of yeast biochar dispersions (10 mg mL^{-1}) was irradiated by sunlight (100 mW cm^{-2}) for 5 min. The temperature variation of the solution was measured by an infrared thermometer. Simultaneously, the same volume of distilled water was used as blank control group.

2.5.2 Photothermal performance of YINCP@EC. In order to further measure that the synthesized particles have excellent light-to-heat conversion performance, 1 mL of deionized water containing a certain amount of CA, YINCP, and YINCP@EC beads were placed into a Petri dish (diameter, 1.5 cm) and then irradiated by sunlight (100 mW cm^{-2}) for 10 min, respectively. An infrared thermometer and an infrared camera were used to monitor the temperature variation and photothermal effect of composites at each time interval.

2.6. Release behavior of IMI

Pesticide-loaded YINCP@EC (5 mg) was soaked in 4 mL of deionized water, NaCl (0.2 g L^{-1}), Na_2SO_4 (0.2 g L^{-1}), or Na_2CO_3 (0.2 g L^{-1}) aqueous solution, and phosphate buffers with pH values of 3, 5, 7, 9, and 11, respectively. After that, the YINCP@EC was irradiated using an analog daylight lamp source (100 mW cm^{-2}) at room temperature. At regular intervals, 0.5 mL of the above supernatants were taken out to be tested by UV-vis spectroscopy and displaced instantly with corresponding fresh buffer. For sunlight-triggered IMI release, YINCP@EC (5 mg) was soaked in 4 mL of deionized water. Then, the beads were exposed to the sunlight for 0.5 h at different time points. At certain time intervals, 0.5 mL of the solution was collected to determine IMI concentration. Meanwhile, 0.5 mL of distilled water was replenished to the system for further irradiation. The same weight of YINCP@EC soaked in the same condition without sunlight irradiation. Ultimately, the IMI release percentage (RP) was calculated by eqn (2):

$$\mathrm{RP}\ (\%) = \frac{C_t V_{\mathrm{total}} + \sum_{0}^{t-1} C_t \times V_t}{m_0} \times 100\% \quad (2)$$

where V_{total} (mL) is the volume of the total solution, and m_0 (μg) is the IMI content in the YINCP@EC before release, C_t (μg mL^{-1}) and V_t (mL) are the IMI concentration and volume of solution taken out at time t, respectively.

2.7. Release kinetics

The release kinetics of IMI from YINCP@EC was analyzed using first-order,[31] Ritger–Peppas,[40–42] and parabolic diffusion[43] models as followed:

$$\ln\left(1 - \frac{M_t}{M_\infty}\right) = -kt \quad (3)$$

$$\frac{M_t}{M_\infty} = kt^n \quad (4)$$

$$\frac{M_t}{M_\infty} = kt^{0.5} + bt \quad (5)$$

where M_t/M_∞ is the fraction of released IMI until time t, b is a constant, k is kinetic constant of release system, and n is the diffusional exponent characteristic to describe the release mechanism.

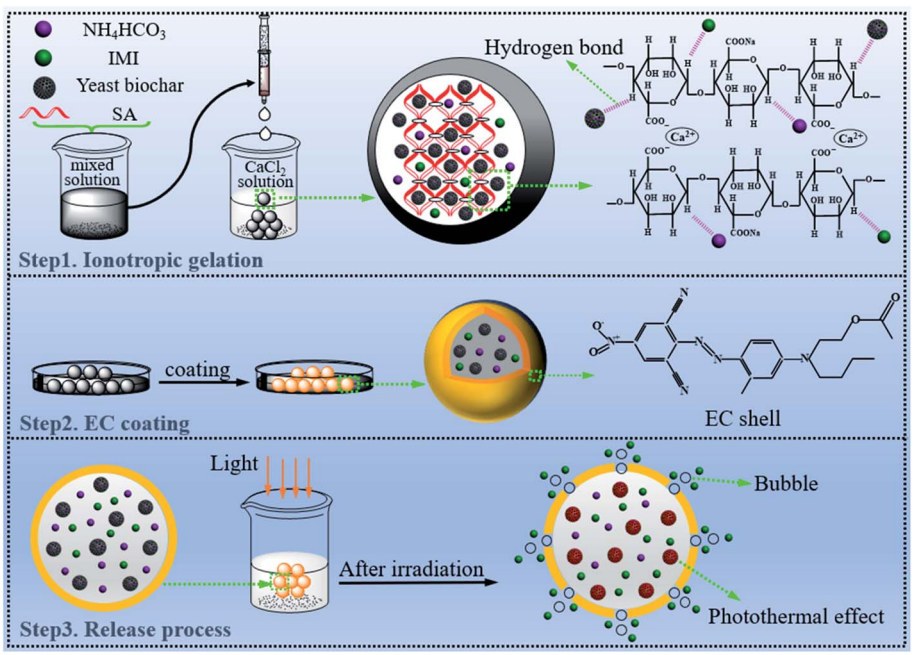

Scheme 1 The proposed mechanism for the formation of the YINCP@EC and its light-triggered release of IMI molecules.

© 2021 The Author(s). Published by the Royal Society of Chemistry

3. Results and discussion

3.1. Preparation and characterization of the YINCP@EC

For minimizing volatilization and leaching of pesticide, and improving its utilization efficiency, we developed a novel intelligent controlled release platform (YINCP@EC) with incorporation of photothermal material yeast biochar, frequently-used pesticide IMI, thermolabile substance NH_4HCO_3, active agent carrier CA, and adhesive coating EC. The detailed fabrication process of YINCP@EC and its controlled release behavior is described in Scheme 1.

In this study, a certain proportion of yeast biochar, NH_4HCO_3, IMI and SA were firstly dispersed in the aqueous solution to form a mixed solution. Since SA can form a sol liquid when dissolved in a solution, its natural viscosity can play a key role in stabilizing yeast biochar, NH_4HCO_3 and IMI. Once the mixed solution was added dropwise into the $CaCl_2$ solution, the beads with good morphology and shape were generated instantaneously because of the chelation between negatively charged $-COO^-$ groups on the skeleton of SA and positively charged Ca^{2+} ions (step 1). Therein, the CA with a network structure acted as a carrier for yeast biochar, IMI and NH_4HCO_3 through hydrogen bond linkage. In the subsequent process (step 2), to further improve the mechanical properties and stability of the composites, the resulting beads was coated by EC to form YINCP@EC after drying. By these means, a smart pesticide carrier system (YINCP@EC) was successfully constructed. In the following release test (step 3), the temperature of YINCP@EC could increase substantially under sunlight irradiation due to the excellent photothermal conversion ability of yeast biochar introduced into the system, which triggered the decomposition of NH_4HCO_3 to generate bubbles (Fig. S1†). Bubbles generated during the decomposition can effectively damage the EC shell, thereby facilitating the entry of water molecules into YINCP@EC, resulting in the pesticide encapsulated in the composites released gradually from the carrier to the solution.

Predicting from their composition, the as-prepared YINCP@EC with excellent pH, photothermal-responsiveness, and high stability could be meaningful for the development of biodegradable, biocompatible and biosafe pesticide-carriers for controlled release of pesticides in potential agricultural application. In more details, the addition of non-toxic CA not only served as a matrix for boning the cargoes through hydrogen bonds, but also endowed the YINCP@EC a pH-responsive controlled release property. Furthermore, the yeast biochar introduced in this sunlight-triggered release platform has great potential compared with other photothermal materials owing to its easy fabrication, low cost, and satisfactory light-to-heat conversion ability. Moreover, the EC shell can further improve the mechanical property of the synthetic sphere, and it is very conducive to actual transportation and application.[44] In summary, the synthetic YINCP@EC combined the structural advantages of CA, yeast biochar, and EC, which have opened an appropriate route for constructing an environmentally friendly light-controlled release of pesticides.

To give further insight of the forming and photothermal-responsive controlled release process, the surface characteristics of samples were investigated in photographs and SEM images, as displayed in Fig. 1. It can be seen from Fig. 1a that the color of the prepared wet beads changed significantly from translucent to milky white, to black, corresponding to CA, blank (mass ratio = 0 : 2 : 4 : 0.5), and YINCP (mass ratio = 3 : 2 : 4 : 0.5), respectively. This color change proves that YINCP has been successfully granulated by ion gelation technique. In Fig. 1b, the yeast biochar microspheres possessed irregular ellipsoid shapes with an average size of ~3 μm and showed a porous surface, which endowed the yeast biochar a large specific surface area. As displayed in Fig. 1c and d, YINCP showed a relatively rough surface, this can be attributed to that the large amount of yeast biochar, NH_4HCO_3 and IMI were wrapped in CA matrix. Moreover, the elemental maps of YINCP (Fig. S2†) showed that C (mainly ascribed to yeast biochar), N (mainly ascribed to NH_4HCO_3), Ca (ascribed to CA), Cl (ascribed to IMI), and Na (ascribed to CA) uniformly distributed in YINCP, further suggesting that yeast biochar, NH_4HCO_3 and IMI were distributed in CA networks. Subsequently, YINCP was well wrapped by EC to form YINCP@EC with a diameter of approximately of 1.5 mm which possessed a smooth surface (Fig. 1e), wherein the EC shell played a key role in hindering the release of IMI. As shown in the cross-section image (Fig. 1f), it can clearly observe the existence of the EC shell. And when YINCP@EC was immersed in water without sunlight irradiation for 30 h, only a few small holes appeared in the coating (Fig. 1g). For comparison, when YINCP@EC was soaked in water under sunlight irradiation for 30 h, the coating was almost completely destroyed, and numerous holes appeared (Fig. 1h). This can be attributed to the fact that yeast carbon can absorb light energy and convert it into heat energy under sunlight irradiation, which quickly raises the temperature of the composites, thereby causing a large amount of NH_4HCO_3 to decompose into CO_2 and NH_3. Bubbles generated during the decomposition can effectively damage the EC shell, so facilitated the IMI release from YINCP@EC.

For acquiring the interactions in YINCP@EC, FTIR measurements were performed. The FTIR spectra of yeast biochar, CA, YINCP and YINCP@EC are demonstrated in Fig. 2a. As shown in curve a, the characteristic absorption peaks of yeast biochar could be observed at 3420, 2920, 2850, 1640 and 1450 cm^{-1}.[37] In curve *b*, the strong peaks at 3430, 1635, and 1425 cm^{-1} were the characteristic absorption peaks of CA.[45] In the spectrum of YINCP, the stretching vibration of –OH, asymmetric and symmetric stretching vibration $-COO^-$ absorptions peak was shifted from 3430, 1635, and 1425 cm^{-1} to 3400, 1630 and 1433 cm^{-1}, respectively, which probably contribute to the formation of hydrogen bond between yeast biochar and CA. Moreover, the newly emerged characteristic peak at 1564 and 1290 cm^{-1} corresponded to the vibration band of N=N in the imidazolidine ring and N–O stretching of the azoxy group, respectively, suggesting that IMI was successful encapsulated in YINCP.[31,46] After modification with EC, a shift from 3400 cm^{-1} to 3352 cm^{-1} was observed, and the peak also became wider, indicating that hydrogen bond was formed between YINCP and EC molecules.[47,48]

The zeta potential analyses were further applied to evaluate the surface characteristics of the YINCP@EC. It is a convenient index which can illustrate the samples surface charge distribution.[49] From Fig. 2b, it can be clearly seen that the yeast biochar exhibited a negative zeta potential (−6.15 mV) due to

© 2021 The Author(s). Published by the Royal Society of Chemistry

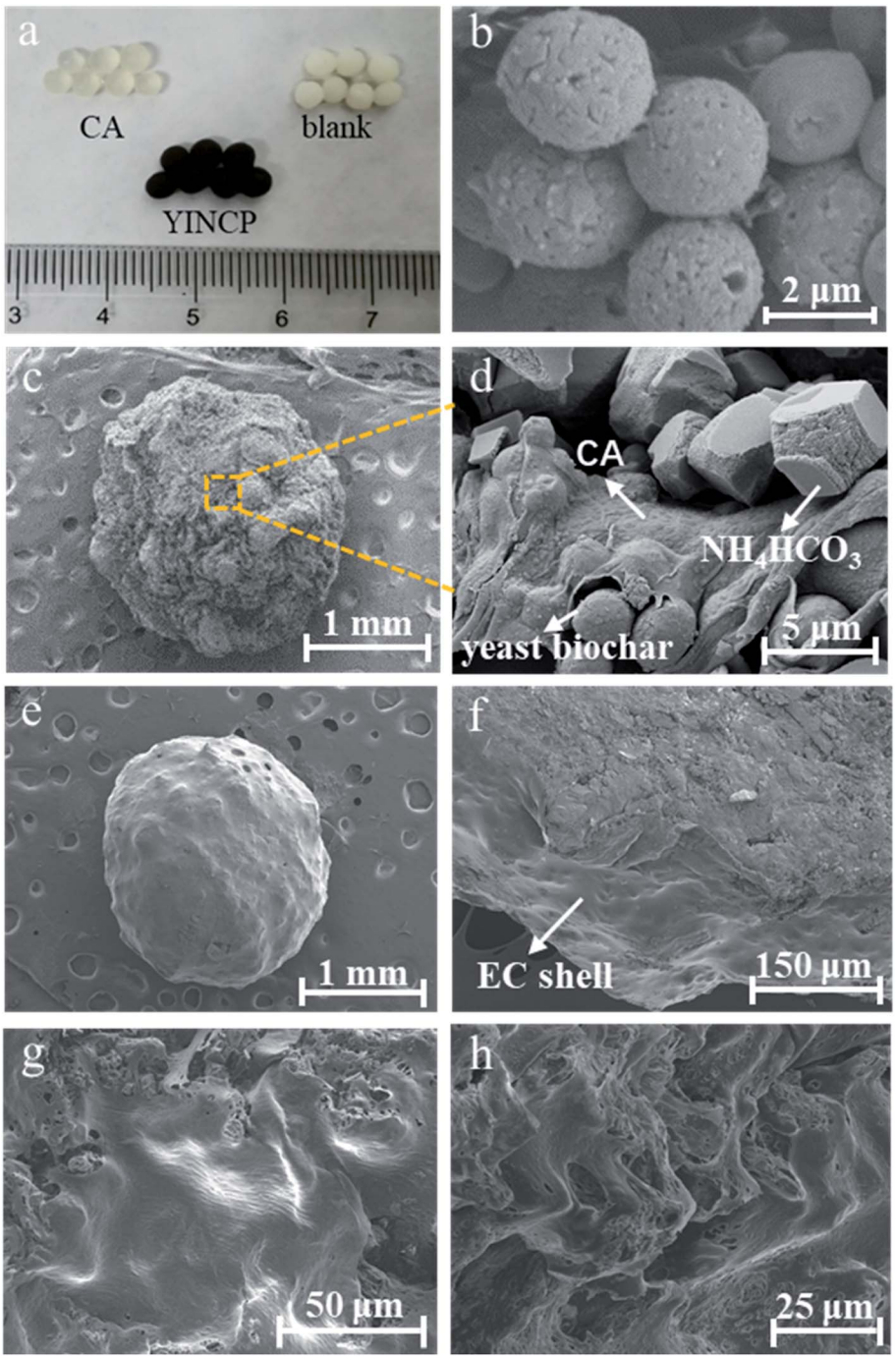

Fig. 1 The appearance of samples (a). SEM images of (b) yeast biochar, (c and d) YINCP (e) YINCP@EC, (f) the cross-section of YINCP@EC, and (g and h) the outer surface of YINCP@EC after release without sunlight and under sunlight irradiation for 30 h.

the negative charges on the surface. And the mean charge of CA was −15.2 mV, which may be attributed to the presence of many –COOH and –OH on the surface of CA.[50] After mixing with CA, NH_4HCO_3 and IMI, the zeta potential altered to be a lower negative value (−16.9 mV), further confirming the adsorption of negatively charged yeast biochar on CA. However, the zeta potential value of YINCP@EC decreased slightly after EC coating, which may be attributed to the presence of acetate groups on the structure of EC molecules.[51] The dissociation of these groups produces a negative charge, which results in a negative zeta potential value.

TGA was also carried out to confirm the successful synthesis of YINCP@EC. The thermographs of yeast biochar, CA, YINCP and YINCP@EC were displayed in Fig. 3. It can be seen from Fig. 3a, the first stage (20–100 °C) of mass loss (4.28%) was ascribed to the loss of physically adsorbed water.[52] The second stage (100–420 °C) of mass loss (32.41%) was attributed to the dehydration of saccharide ring and the fracture of C–O–C glycoside

© 2021 The Author(s). Published by the Royal Society of Chemistry

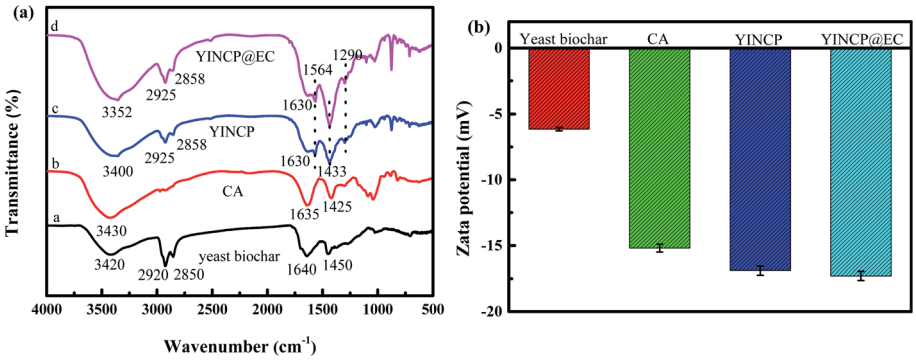

Fig. 2 (a) FTIR spectra, (b) zeta potential (1.0 mg mL^{-1}) of yeast biochar, CA, YINCP and YINCP@EC.

bond of yeast.[53] The third stage (420–700 °C) of mass loss (61.58%) was assigned to the intermolecular crosslinking of oligosaccharides by dehydration at higher temperatures. In contrast, the multiple degradation profiles of CA, YINCP and YINCP@EC were rather similar, all the degradation process can be divided into four stages. The remaining mass percentage of YINCP (22.81%) was slightly lower than of CA (23.19%), which was due to the addition of yeast carbon and decomposition of NH_4HCO_3. Moreover, the residue mass of YINCP@EC (Fig. 3d) was measured to be as low as 12.61% in the same temperature range, which can be attributed to the decomposition of EC shell.[54]

3.2. Stability investigation

The structural stability performance of YINCP@EC in aqueous solution was studied. As can be seen in Fig. 4, there are some bubbles appeared on the surface of YINCP@EC when it was immersed in the aqueous solution at room temperature. With prolonging the immersion time, the bubbles on the surface of the material increased slowly. The appearance of these bubbles is due to the unstable NH_4HCO_3 added to the system, which can be decomposed into CO_2 and NH_3 in a small amount at room temperature. In Fig. 4, it is easy to figure out that YINCP@EC was rather stable in aqueous solution and consistently kept the spherical shape. The collapse ratio of YINCP@EC increased slowly with time and reached only 8.5% after 60 days, suggesting that the composite was quite stable in aqueous solution. This could be attributed to the hydrophobic EC coating which can availably block the entrance of water molecules into YINCP@EC. Such a high stability promotes the extended application of YINCP@EC in the agricultural field.

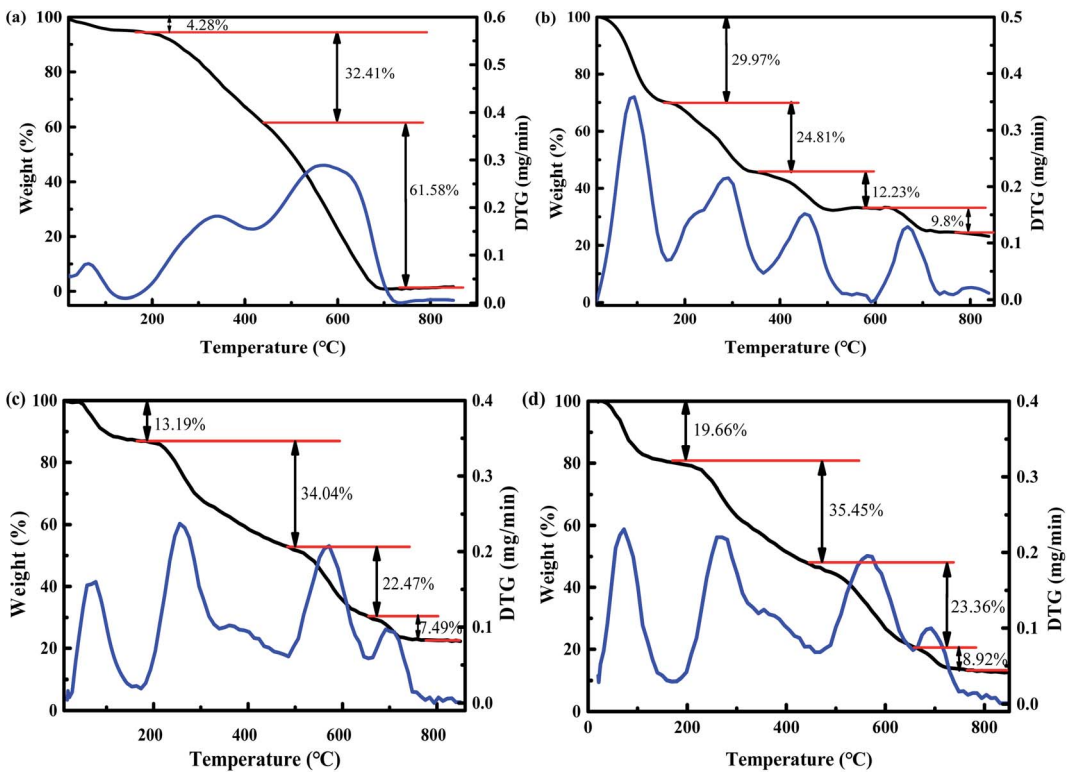

Fig. 3 Thermographs of yeast biochar (a), CA (b), YINCP (c) and YINCP@EC (d).

© 2021 The Author(s). Published by the Royal Society of Chemistry

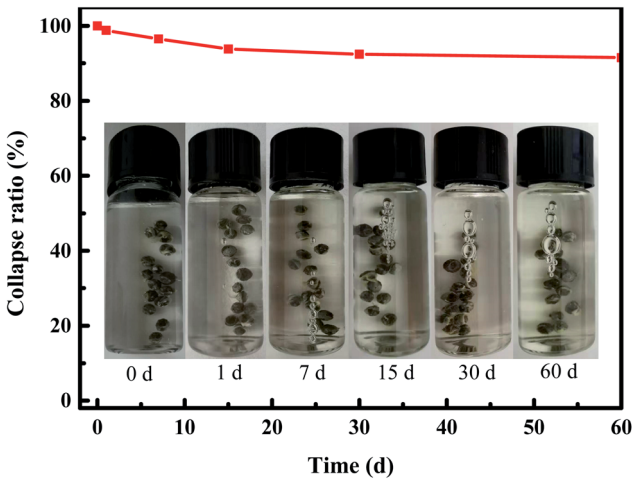

Fig. 4 Structural stability of YINCP@EC with time. (Inset: digital images of YINCP@EC in aqueous solution after 0 d, 1 d, 7, 15, 30, and 60 d, respectively.)

3.3. Photothermal performance of yeast biochar

To confirm the light absorption capability of samples, the UV-vis diffuse reflectance spectra of CA, yeast biochar and YINCP@EC were performed. It can be shown in Fig. 5a, the yeast biochar showed a high absorption capacity for the light (across the UV and visible regions), which has the potential to be an excellent photothermal conversion agent, while CA exhibited relatively limited light absorption ability. In addition, it is obvious that YINCP@EC preserves nearly 90% of the light absorption capacity of yeast carbon, indicating blending materials does not inhibit the light absorption of yeast biochar. Such excellent light absorption of YINCP@EC lays a foundation for the conversion of light into heat, which is expected to realize the controlled release of IMI from composite.

It is necessary to evaluate the photothermal conversion ability of yeast biochar under sunlight irradiation to further verify its potential as photothermal-responsive materials. In Fig. 5b, the temperature of pure water did not change significantly after being irradiated with the sunlight for 5 min. However, the temperature of the yeast biochar aqueous solution (10 mg mL^{-1}) rose rapidly to 35.1 °C at the same time interval. In addition, it can be clearly observed that the inner wall of the cuvette containing the yeast biochar aqueous dispersion showed obvious water droplets after 5 min of irradiation (the inset image of Fig. 5b). These results confirm that yeast biochar can effectively convert photon energy into heat energy.

For further illustrating that the presence of the EC coating does not affect the photothermal conversion performance of the

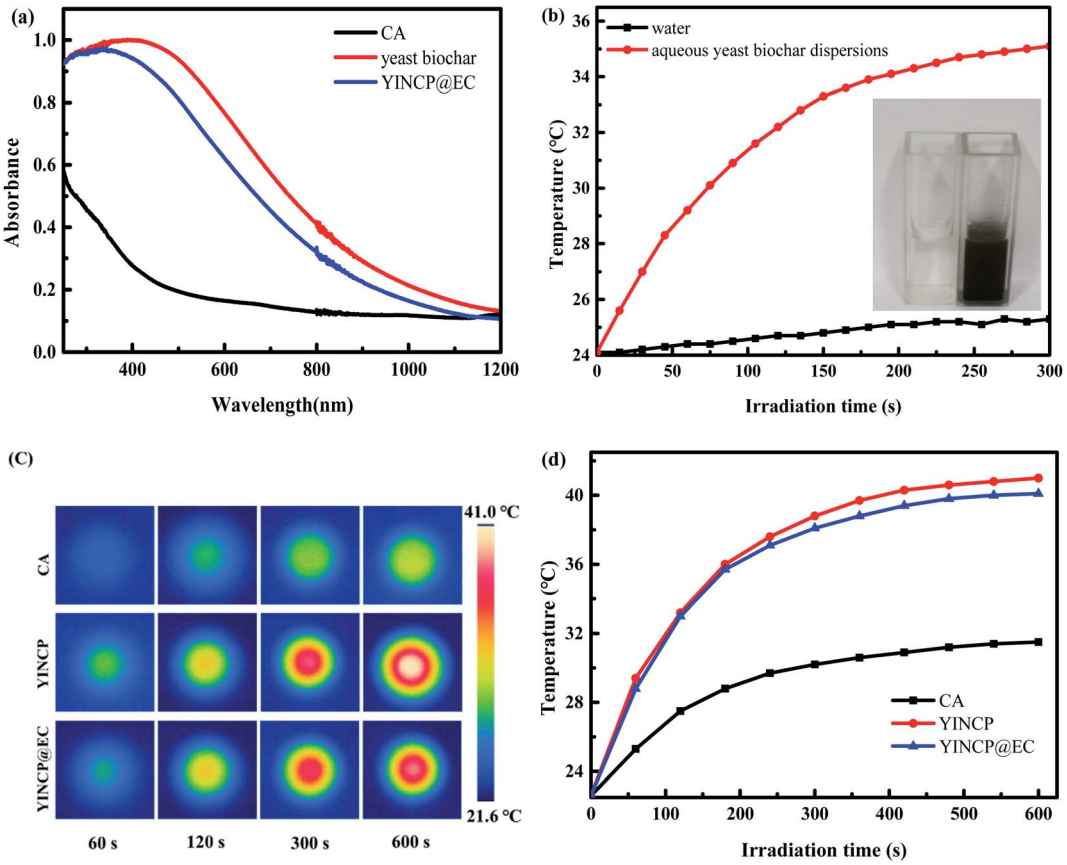

Fig. 5 (a) UV-vis diffuse reflectance spectra of yeast biochar, CA and YINCP@EC. (b) Temperature changes of pure water and 10 mg mL^{-1} aqueous yeast biochar solutions under irradiation with the sunlight of 100 mW cm^{-2}. (Inset: photograph of aqueous yeast biochar solutions and distilled water after 300 s of irradiation.) (c) infrared thermal images of samples at the various times under sunlight irradiation of 100 mW cm^{-2} and (d) corresponding temperature profiles.

© 2021 The Author(s). Published by the Royal Society of Chemistry

beads, the temperature of CA, yeast biochar and YINCP@EC was detected by an infrared camera, and the results are displayed in Fig. 5c and d. It can be seen that the temperature of YINCP and YINCP@EC beads rose rapidly after being irradiated with 100 mW cm^{-2} of sunlight. After 10 minutes, the temperature of YINCP@EC and YINCP beads increased by 17.5 °C and 18.4 °C, respectively. As a comparison, under the same irradiation conditions, the temperature of CA beads was not change significantly, which confirms that the obtained YINCP@EC has satisfactory photothermal performance and the EC coating shell layer does not affect its performance.

3.4. Release behavior of IMI

To evaluate the photothermal-responsive release properties of the YINCP@EC, we chose the IMI as a model pesticide. The causes lie in that IMI as a model pesticide has widespread applications in modern agriculture (for more than 140 field crops).[38] In succeeding experiments, the test of release efficiency of IMI was conducted at different yeast biochar mass ratio and external buffer solutions, as shown in Fig. 6 and 7.

Due to the diverse surface properties of YINCP@EC prepared at various weight ratio of yeast biochar, the YINCP@EC behaved differently in release IMI efficiency. The release behavior of IMI from YINCP@EC was performed in water at different ratio under sunlight, and the profiles are depicted in Fig. 6a. It can be seen that the amount of IMI released from YINCP@EC increased with increasing the content of yeast biochar. This can be attributed to the fact that the temperature of the synthesized particles increased significantly with the increase of yeast carbon content, thereby accelerating the decomposition of NH_4HCO_3. Then, the holes caused by the bubbles generated by decomposition facilitated the entry of water molecules into YINCP@EC, which resulted in the pesticide encapsulated in the composites released gradually from the adsorbent to the solution. In comparison, the release percentage of IMI decreased slightly with adding excessive yeast biochar, which may be attributed to that a certain of IMI molecules were adsorbed on the increased yeast biochar with porous surface. The acquired results prove that the YINCP@EC mass ratio ($W_{\text{yeast biochar}}/W_{CA} = 3:2$) had the best performance of the photothermal-responsively controlled release. Apparently, after yeast biochar modification, the YINCP@EC exhibited a more obvious sunlight-induced BNOA release property, which may be owing to the remarkable photothermal effect of yeast biochar in YINCP@EC. In addition, we analyzed the functional groups of the YINCP@EC after the release of IMI by FT-IR. As shown in Fig. S3,† the characteristic peak of IMI at 1564 and 1290 cm^{-1} were disappeared, suggesting that IMI was successfully released from YINCP.

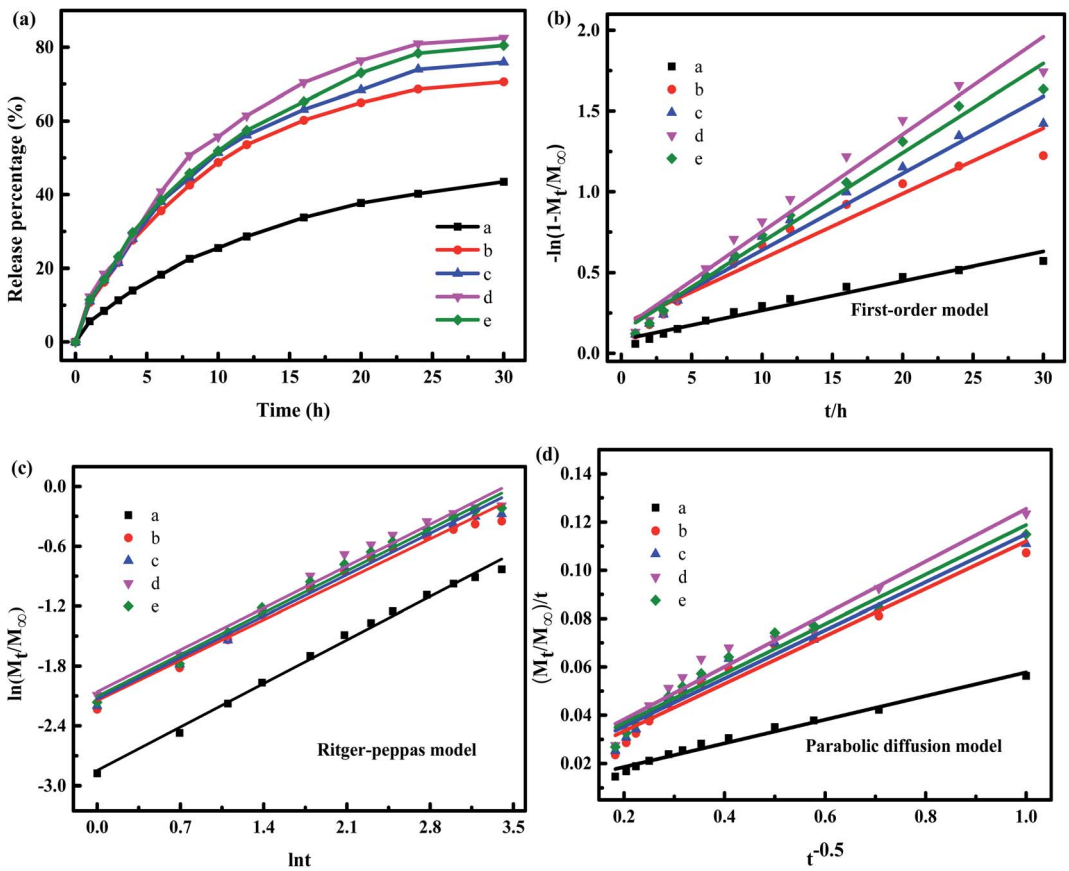

Fig. 6 (a) Release curves of YINCP@EC with different mass ratios (a – 0 : 2 : 4 : 0.5, b – 1 : 2 : 4 : 0.5, c – 2 : 2 : 4 : 0.5, d – 3 : 2 : 4 : 0.5 and e – 4 : 2 : 4 : 0.5) under irradiation of sunlight of 100 mW cm^{-2}, plots of different kinetic models for the release of IMI from the YINCP@EC compounds: (b) first-order model, (c) Ritger–Peppas model, (d) parabolic diffusion model.

© 2021 The Author(s). Published by the Royal Society of Chemistry

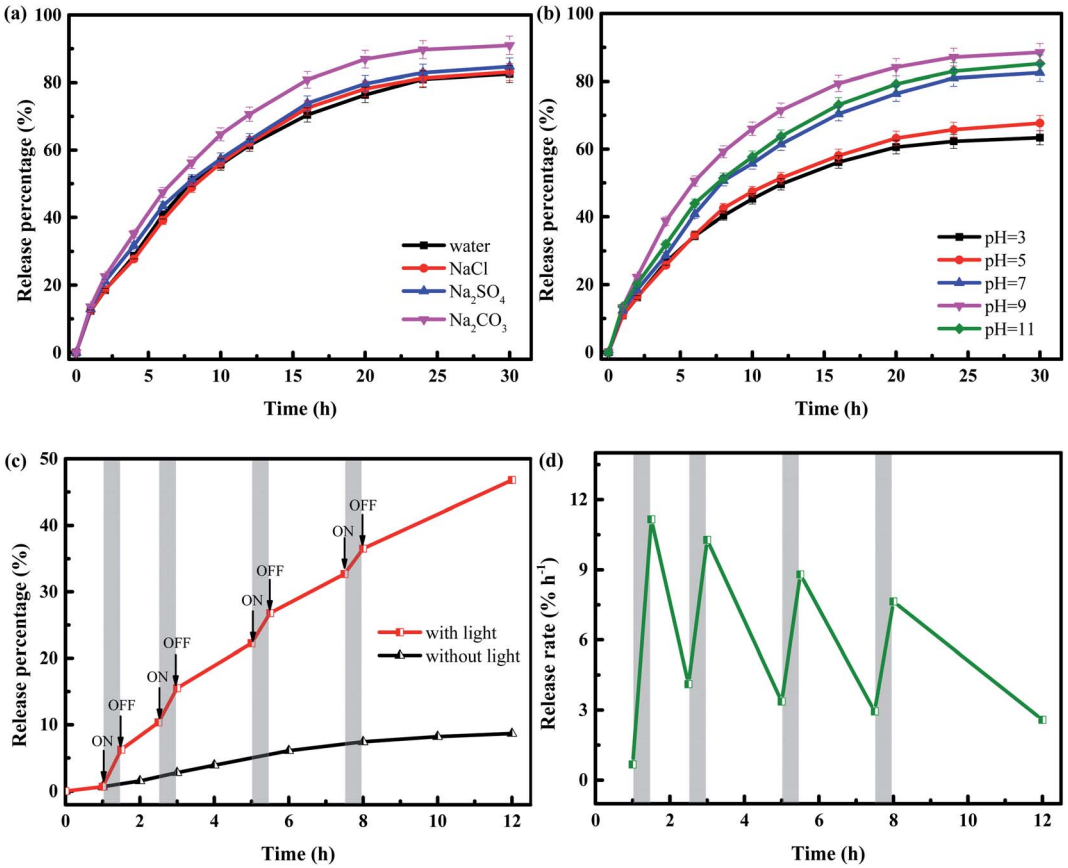

Fig. 7 Influence of (a) coexisting ions and (b) pH on IMI release of IMI from YINCP@EC in water. (c) Cumulative release profiles of IMI from YINCP@EC with and without light irradiation (100 mW cm^{-2}). (d) Calculated IMI release rate from YINCP@EC for repeated sunlight on–off cycles.

In order to further explore the release mechanism of IMI from YINCP@EC, the release kinetic models including first-order, Ritger–Peppas and parabolic diffusion models were applied to fit the measured sunlight-triggered release data and the results are shown in Fig. 6b–d. Typically, the first-order formula illustrates that the release process depended on both disintegration and ion-exchange step. The Ritger–Peppas expression is used to explain drug diffusion and swelling of YINCP@EC. The value of $n < 0.45$ corresponds to the drug diffusion control, $n > 0.89$ is attributed to the swelling-controlled drug release; $0.45 < n < 0.89$ is due to the cooperation of drug diffusion and swelling of YINCP@EC. The parabolic diffusion equality indicates that the drug release procedure belongs to an external surface diffusion process. The values of parameters and regression coefficients (R^2) were presented in Table 1.

As can be seen in Table 1, the values of R^2 calculated by the Ritger–Peppas model are higher than the other two models in all the cases, suggesting that the Ritger–Peppas model can better explain the release mechanism of IMI from YINCP@EC. Additionally, the values of the diffusion exponent n were larger than 0.45 and lower than 0.89, indicating that the IMI release from the composites was controlled by both a diffusion of drug and swelling of spheres.

The release efficiency of pesticides is often drastically affected by the ions in the aqueous solution. Considering the effect of coexisting ions, the release behaviors of IMI from YINCP@EC were performed in different salt solution of NaCl,

Table 1 The corresponding rate constants of YINCP@EC fitting to different kinetic models

	First-order model		Ritger–Peppas model			Parabolic diffusion model	
Sample	R^2	k	R^2	K	n	R^2	k
a	0.9616	0.01822	0.99366	0.0579	0.62326	0.97815	0.04904
b	0.94475	0.04057	0.97837	0.1168	0.57916	0.95872	0.09827
c	0.96418	0.04764	0.98014	0.1187	0.59334	0.95794	0.09963
d	0.96851	0.0604	0.97823	0.1277	0.59967	0.96023	0.10894
e	0.98077	0.05535	0.9852	0.1219	0.59906	0.96181	0.10253

© 2021 The Author(s). Published by the Royal Society of Chemistry

Na_2SO_4 and Na_2CO_3 (0.2 g L^{-1}) under the room temperature with the sunlight of 100 mW cm^{-2}, respectively. As shown in Fig. 7a, the release of IMI in the former two solution displayed similar behaviors compared in the solution of distilled water, indicating that Cl^-, SO_4^{2-} posed little impact on the release of IMI from YINCP@EC. Differently, CO_3^{2-} showed a slightly positive effect on the release of IMI from YINCP@EC, which was probably due to the addition of Na_2CO_3 increased the pH of the solution, leading to the ionization of –COOH and the enhancement of repulsive force, thereby promoting the release of IMI. In brief, the YINCP@EC showed high stability against coexisting ions.

Besides, the influence of pH on the release of IMI from YINCP@EC was also explored and shown in Fig. 7b. It can be seen that the release percentage of IMI showed a downward trend in the range of pH 3–7, and then increased with increasing pH to 9. This is because the CA and yeast biochar molecule added to the release system have abundant –COOH hydrophilic groups. Under acidic conditions (pH < 7), most $–COO^-$ could bind with hydrogen ions to form –COOH, which weaken the electrostatic repulsion between the anionic groups, thereby inhibiting the swelling of the YINCP@EC beads and hindering the release of IMI molecules loaded in the composites.[55,56] Under alkaline conditions (pH > 7), more –COOH were ionized, which enhanced the repulsive force, leading to the further expansion of polymer matrix and accelerating the release of IMI. However, when the pH further increased to 11, the release percentage of IMI slightly decreased. This can be ascribable to the weakening of electrostatic repulsive force between the $–COO^-$, which results from the existence of electrostatic attraction of Ca^{2+} with other counter ions, thereby shrinking the polymer chain. This unique pH-sensitive release behavior of YINCP@EC allows it to be used as a pH-triggered pesticide delivery platform, which has broad application prospects in modern agriculture.

To further confirm the ability of sunlight to trigger the IMI release, we tested the release percentage of IMI from YINCP@EC under intermittent sunlight irradiation and in dark condition, and the results were showed in Fig. 7c. Under dark conditions, the release percentage of IMI rose slowly over time, suggesting that IMI molecules gradually dispersed from the matrix into the surrounding media, and the accumulative release of IMI finally reached an equilibrium value of 8.69% within 12 h. This can be explained by the fact that NH_4HCO_3 is not very stable and can be decomposed in a small amount at room temperature. When the beads were under sunlight irradiation, the release percentage of IMI increased significantly. The enhanced sunlight-triggered IMI release can be attributed to that the yeast biochar absorbed in the network-structured of YINCP@EC matrix can effectively convert sunlight energy into thermal energy. The release rate profile of IMI vividly exhibited sunlight-dependent behavior of YINCP@EC, as shown in Fig. 7d. The measured release rate was 11.16% h^{-1} under first irradiation, rapidly decreasing to 4.11% h^{-1} after 2 h of treatment in the dark while rising again to 10.28% h^{-1} during the second cycle and remarkably reducing under the shady condition. This IMI release pattern suggests that the YINCP@EC have sustained photothermal-responsive capacity and that the release rate of IMI can be controlled by switching sunlight irradiation.

4. Conclusion

In summary, a simple and promising pesticide particle (YINCP@EC) was developed by the combination of yeast biochar, IMI, NH_4HCO_3, CA, and EC. This novel photothermal-responsive controlled-release platform can regulate the IMI release rate through switching light irradiation due to the excellent sunlight-to-heat conversion ability of yeast biochar. Sunlight irradiation can effectively increase the temperature of YINCP@EC, hereby causing a large amount of NH_4HCO_3 decomposed to CO_2 and NH_3 to form numerous holes in the EC coating. The holes may effectively facilitate the release of IMI from YINCP@EC. Furthermore, the EC coating could enhance the mechanical property of the synthetic YINCP@EC, greatly benefiting the reduction of IMI loss and enhancement of utilization efficiency. Additionally, YINCP@EC showed unique pH-sensitivity and high stability. Hence, this sunlight-triggered yeast biochar-based photothermal-responsive platform provides a promising way for the controlled release of IMI, and may have broad application prospects in the agricultural field.

Conflicts of interest

There are no conflicts to declare.

Acknowledgements

This work was supported by the Natural Science Basic Research Program of Shaanxi (Program No. 2021SF-497), and the Fundamental Research Funds for the Central Universities, CHD 300102291403.

References

1 M. Raileanu, L. Todan, M. Crisan, A. Braileanu, A. Rusu, C. Bradu, A. Carpov and M. Zaharescu, *J. Environ. Prot.*, 2010, **01**, 302–313.
2 X. Xu, B. Bai, H. Wang and Y. Suo, *ACS Appl. Mater. Interfaces*, 2017, **9**, 6424–6432.
3 B. Liu, C. Chen, R. Wang, S. Dong, J. Li, G. Zhang, D. Cai, S. Zhai and Z. Wu, *ACS Sustainable Chem. Eng.*, 2019, **7**, 14924–14932.
4 Y. Gao, Y. Zhang, S. He, Y. Xiao, X. Qin, Y. Zhang, D. Li, H. Ma, H. You and J. Li, *Chem. Eng. J.*, 2019, **364**, 361–369.
5 M. C. Camara, E. V. R. Campos, R. A. Monteiro, A. do Espirito Santo Pereira, P. L. de Freitas Proenca and L. F. Fraceto, *J. Nanobiotechnol.*, 2019, **17**, 100.
6 Y. Gao, A. E. Kaziem, Y. Zhang, Y. Xiao, S. He and J. Li, *Microporous Mesoporous Mater.*, 2018, **255**, 15–22.
7 S. Feng, J. Wang, L. Zhang, Q. Chen, W. Yue, N. Ke and H. Xie, *Polymer*, 2020, **12**, 2268.
8 Z. Shen, H. Wen, H. Zhou, L. Hao, H. Chen and X. Zhou, *Mater. Sci. Eng., C*, 2019, **105**, 110073.

© 2021 The Author(s). Published by the Royal Society of Chemistry

9 I. Ravier, E. Haouisee, M. Clement, R. Seux and O. Briand, *Pest Manage. Sci.*, 2005, **61**, 728–736.
10 L. Hao, L. Gong, L. Chen, M. Guan, H. Zhou, S. Qiu, H. Wen, H. Chen, X. Zhou and M. Akbulut, *Chem. Eng. J.*, 2020, **396**, 125233.
11 C. Xu, L. Cao, P. Zhao, Z. Zhou, C. Cao, F. Zhu, F. Li and Q. Huang, *Int. J. Mol. Sci.*, 2018, **19**, 854.
12 S. Song, Y. Wang, J. Xie, B. Sun, N. Zhou, H. Shen and J. Shen, *ACS Appl. Mater. Interfaces*, 2019, **11**, 34258–34267.
13 K. Ding, L. Shi, L. Zhang, T. Zeng, Y. Yin and Y. Yi, *Polym. Chem.*, 2016, **7**, 899–904.
14 Y. Shan, L. Cao, B. Muhammad, B. Xu, P. Zhao, C. Cao and Q. Huang, *J. Colloid Interface Sci.*, 2020, **566**, 383–393.
15 S. B. Lao, Z. X. Zhang, H. H. Xu and G. B. Jiang, *Carbohydr. Polym.*, 2010, **82**, 1136–1142.
16 M. E. Taverna, C. A. Busatto, M. R. Lescano, V. V. Nicolau, C. S. Zalazar, G. R. Meira and D. A. Estenoz, *J. Hazard. Mater.*, 2018, **359**, 139–147.
17 Y. Liang, M. Guo, C. Fan, H. Dong, G. Ding, W. Zhang, G. Tang, J. Yang, D. Kong and Y. Cao, *ACS Sustainable Chem. Eng.*, 2017, **5**, 4802–4810.
18 A. E. Kaziem, Y. Gao, Y. Zhang, X. Qin, Y. Xiao, Y. Zhang, H. You, J. Li and S. He, *J. Hazard. Mater.*, 2018, **359**, 213–221.
19 X. Wang and J. Zhao, *J. Agric. Food Chem.*, 2013, **61**, 3789–3796.
20 M. Guo, W. Zhang, G. Ding, D. Guo, J. Zhu, B. Wang, D. Punyapitak and Y. Cao, *RSC Adv.*, 2015, **5**, 93170–93179.
21 P. Qin, X. Xu, Y. Cai, B. Bai, H. Wang and Y. Suo, *RSC Adv.*, 2017, **7**, 32777–32785.
22 Y. Chi, G. Zhang, Y. Xiang, D. Cai and Z. Wu, *ACS Sustainable Chem. Eng.*, 2017, **5**, 4969–4975.
23 Y. Liu, Y. Sun, G. Ding, Q. Geng, J. Zhu, M. Guo, Y. Duan, B. Wang and Y. Cao, *J. Agric. Food Chem.*, 2015, **63**, 4263–4268.
24 C. Chen, G. Zhang, Z. Dai, Y. Xiang, B. Liu, P. Bian, K. Zheng, Z. Wu and D. Cai, *Chem. Eng. J.*, 2018, **349**, 101–110.
25 H. Chen, Y. Lin, H. Zhou, X. Zhou, S. Gong and H. Xu, *J. Agric. Food Chem.*, 2016, **64**, 8095–8102.
26 Y. Zhang, W. Chen, M. Jing, S. Liu, J. Feng, H. Wu, Y. Zhou, X. Zhang and Z. Ma, *Chem. Eng. J.*, 2019, **361**, 1381–1391.
27 J. Xing, W. Dang, J. Li and J. Huang, *Colloids Surf., B*, 2021, **204**, 111776.
28 B. Gong, Y. Shen, H. Li, X. Li, X. Huan, J. Zhou, Y. Chen, J. Wu and W. Li, *J. Nanobiotechnol.*, 2021, **19**, 41.
29 K. Wang, C. F. Li, Y. Li, J. J. Wang and A. Q. Ma, *Mater. Res. Express*, 2020, **7**, 8.
30 C. Xu, Y. Shan, M. Bilal, B. Xu, L. Cao and Q. Huang, *Chem. Eng. J.*, 2020, **395**, 125093.
31 L. Zhang, S. Ren, C. Chen, D. Wang, B. Liu, D. Cai and Z. Wu, *Chem. Eng. J.*, 2020, **411**, 127881.
32 S. Sharma, S. Singh, A. K. Ganguli and V. Shanmugam, *Carbon*, 2017, **115**, 781–790.
33 Z. Guan, L. Liu, L. He and S. Yang, *J. Hazard. Mater.*, 2011, **196**, 270–277.
34 F. Zhao, Y. Guo, X. Zhou, W. Shi and G. Yu, *Nat. Rev. Mater.*, 2020, **5**, 388–401.
35 L. Zhang, B. Bai, N. Hu and H. Wang, *Sol. Energy Mater. Sol. Cells*, 2021, **221**, 110876.
36 X. Yang, G. Jin, Z. Gong, H. Shen, Y. Song, F. Bai and Z. K. Zhao, *Bioresour. Technol.*, 2014, **158**, 383–387.
37 S. Chen, B. Bai, Y. He, N. Hu, H. Wang and Y. Suo, *RSC Adv.*, 2019, **9**, 1151–1164.
38 D. Drobne, M. Blazic, C. A. Van Gestel, V. Leser, P. Zidar, A. Jemec and P. Trebse, *Chemosphere*, 2008, **71**, 1326–1334.
39 D. Ni, L. Wang, Y. Sun, Z. Guan, S. Yang and K. Zhou, *Angew. Chem., Int. Ed.*, 2010, **49**, 4223–4227.
40 B. Liu, Y. Wang, F. Yang, X. Wang, H. Shen, H. Cui and D. Wu, *Colloids Surf., B*, 2016, **144**, 38–45.
41 A. Bortolin, F. A. Aouada, L. H. Mattoso and C. Ribeiro, *J. Agric. Food Chem.*, 2013, **61**, 7431–7439.
42 A. Olad, H. Gharekhani, A. Mirmohseni and A. Bybordi, *J. Polym. Res.*, 2016, **23**, 241.
43 C. F. Dai, D. Y. Tian, S. P. Li and X. D. Li, *Mater. Sci. Eng., C*, 2015, **57**, 272–278.
44 K. Wasilewska and K. Winnicka, *Materials*, 2019, **12**, 3386.
45 H. S. Samanta and S. K. Ray, *Carbohydr. Polym.*, 2014, **99**, 666–678.
46 G.-P. Lim and M. S. Ahmad, *J. Ind. Eng. Chem.*, 2017, **56**, 382–393.
47 T. F. Yang and X. W. Li, *Korean J. Chem. Eng.*, 2008, **25**, 1201–1204.
48 S. E. El-Habashy, A. N. Allam and A. H. El-Kamel, *Int. J. Nanomed.*, 2016, **11**, 2369–2380.
49 A. E. Ofomaja and Y. S. Ho, *J. Hazard. Mater.*, 2007, **139**, 356–362.
50 D. G. Ahn, J. Lee, S. Y. Park, Y. J. Kwark and K. Y. Lee, *ACS Appl. Mater. Interfaces*, 2014, **6**, 22069–22077.
51 S. M. Mirabedini, I. Dutil and R. R. Farnood, *Colloids Surf., A*, 2012, **394**, 74–84.
52 D. Zheng, B. Bai, X. Xu, Y. He, S. Li, N. Hu and H. Wang, *RSC Adv.*, 2019, **9**, 27961–27972.
53 D. Feng, B. Bai, H. Wang and Y. Suo, *J. Polym. Environ.*, 2017, **26**, 567–588.
54 A. Ouarga, H. Noukrati, I. Iraola-Arregui, A. Elaissari, A. Barroug and H. Ben youcef, *Prog. Org. Coat.*, 2020, **148**, 105885.
55 A. K. Bajpai and A. Giri, *Carbohydr. Polym.*, 2003, **53**, 271–279.
56 H. El-Hamshary, *Eur. Polym. J.*, 2007, **43**, 4830–4838.

© 2021 The Author(s). Published by the Royal Society of Chemistry